

# Separating Parts from 2D Shapes using Relatability

Xiaofeng Mi and Doug DeCarlo  
Rutgers University

Department of Computer Science & Center for Cognitive Science

## Abstract

*It's often important to analyze shapes as made up of parts. But there are two ways to think of how parts fit together. We can characterize the remainder of a shape after a part is removed; here we want to cut the shape so what remains has the simplest possible structure. Alternatively, we can cut out the part so that the part itself takes on a simple shape. These cuts do not directly give rise to a segmentation of the shape; a point inside the shape may associate with the part, the remainder, neither, or both.*

*We present a new model for reconstructing these cuts based on the differential geometry of smoothed local symmetries. The model takes into account relatability (which characterizes clean cuts) to determine part boundaries. Our approach complements and unifies existing work on part-based segmentation of shape, and can be used to construct interesting simplifications of shapes.*

## 1. Introduction

Perception research strongly suggests that the human visual system interprets and represents the shapes of objects by organizing them into perceptual parts [8, 25]. This insight has been the inspiration for a range of approaches in computer vision for analyzing the part structure of 2D shapes [16, 21, 23]. A common theme in this work is the specification of computations that analyze a shape into a hierarchy by partitioning it based on its part structure. In these schemes, each point inside the shape belongs to exactly one part, and the parts themselves are composed together into a tree which groups primitive parts naturally into progressively larger complex structured shapes. These schemes provide an exciting foundation for higher-level processes such as object recognition.

Psychophysical research also suggests an alternative conception of how people see parts in shape, however. Koenderink and van Doorn [14], for example, observe that artists conceptualize shapes as though all the significant parts are elliptical regions, while the hyperbolic patches that connect these parts is insignificant “glue”. Hoff-

man and Richards's characterization of *transversality* [8]—according to which the perceptual system understands some articulated objects as complexes of overlapping and interpenetrating elliptical parts—appeals to a similar principle. This view of parts leads to an analysis of shape in which parts do not directly give rise to a segmentation of the shape. A point inside the shape may associate with exactly one part, with multiple parts, or with no part at all.

Figure 1 illustrates the difference between the two conceptions of part structure. It shows two ways of understanding a fish-shape as built from a body and a tail. The segmentation of Figure 1(b) analyzes each point on the shape either as part of the body or as part of the tail. This is the typical approach for shape analysis in computer vision. The analysis of Figure 1(c), in contrast, describes the body and the tail as elliptical masses glued together along their boundary by a hyperbolic transition region. In Figure 1(c), the fish is body plus tail, but not every point in the fish comes from the body or the tail. This conception of object structure is more common in CAD and computer graphics [10, 19] in applications that construct models from parts. Accordingly, we believe that vision techniques that recognize this part structure have a key role to play in a range of interactive applications, such as interfaces for sketching, manipulating and depicting shape.

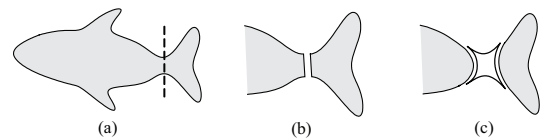


Figure 1. Two ways of analyzing a fish-shape into its body and tail.

This paper offers the first computational investigation of 2D shape analysis that allows for transitions between parts. We make three contributions.

- We introduce a computational model that describes the extent and the prominence of the transition areas between a part and the rest of the shape.
- We show that the idea of transitions between parts gives rise to a unified mathematical characterization of

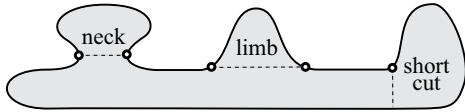


Figure 2. Part structure examples

local shape organization. In particular, it distinguishes extended wholes uniformly from various assemblies of parts, such as limbs, necks, and short-cuts.

- We provide an implementation of our model, based on smoothed local symmetry, and illustrate its applicability in interfaces for shape through a study of sequenced deletion of parts.

The key to our approach is *relatability*, a measure of how easily two separate curve segments at different locations in space can be joined together into a single smooth curve. Relatability is typically invoked to explain contour completion behind an occluder [11, 24]. Our approach is to find part boundaries that cut through corresponding points across a local symmetry axis. We place them where the relatability increases quickly, suggesting that we have moved through a transition region to a natural part. This combination of symmetry and relatability allows us to work with simple and robust clear cases of the general definition of relatability and to build on work on part-based segmentation using symmetry.

After a review of related work, we summarize our approach in Section 2. Then we derive mathematical characterizations of local symmetries (Section 3) that are relevant for modeling boundary strength (Section 4). Then we describe our implementation (Section 5) and discuss our results.

### 1.1. Related Work

A common computational approach to shape representation is to infer a skeleton that describes the local symmetries of the shape [2, 4, 13, 22]. These representations enjoy a convergence with psychophysical models [15], and also form the basis of much of the work on the computation of part structure. Approaches based on local symmetries can locate parts by detecting singularities (shocks) in the entropy scale space of the shape [13]—a formalism that operationalizes the use of symmetry and size to guide part decomposition.

These skeletal models can be improved by taking into account the boundary of the shape. In general, negative curvature minima are likely boundaries between perceptual parts [8], and De Winter and Wagemans [5] have shown through psychophysical studies that parts crucially depend both on the boundary and on region geometry. The computational approach of Siddiqi and Kimia [23] achieves this by using symmetry axes to find one kind of part—*necks*—and using boundary curvature to find another kind of part—*limbs*.

Singh et al. [26] further argue for a *short-cut* rule involving both boundaries and regions: these cuts hit a single local curvature minimum but cross a local axis of symmetry. These three types of connections are shown in Figure 2. Our approach continues this tradition of exploiting both region and boundary information to describe part structure.

All of the prior approaches partition shapes into pairs of parts using a single cut that connects two distinct points on the boundary with a line or curve that remains inside the shape—as shown in Figure 1(a) and (b). Rom and Medioni [21] do recognize that a transition region must be adjusted to remove parts cleanly, but they assume that transitions are located in fixed locations around prespecified part boundaries. Their model is good enough to find new symmetries in simplified shapes—an insight we draw from their approach—but we greatly simplify and generalize this insight by modeling transitions explicitly. Junctions between parts have been described as well. Blum and Nagel [3] define *ligatures* as portions of the symmetry axis that represent segments of the boundary with negative curvature. August et al. [1] further analyze ligatures to develop more stable descriptions using the medial axis, by simply ignoring the ligatures when forming the parts. Our approach goes beyond this by characterizing parts in a smooth and uniform way using relatability. We revisit these considerations after we present our model.

## 2. Our Approach

Here we summarize our approach for separating parts from shapes. Working from the differential geometry of smoothed local symmetries, we can identify reasonable locations to cut the shape so that when a part is removed, no trace of it remains on the rest of the shape. We can do the same for the part itself, so that it takes on a simple shape. Thus, our approach aims to ignore the transitional region of the shape between the part and the rest of the shape—see Figure 1(c). The remainder of this section describes smoothed local symmetries [4], and our methodology for locating cuts.

### 2.1. Smoothed Local Symmetries (SLS)

Axial representations [22] describe local symmetries in terms of a generator that sweeps along the symmetry axis. For smoothed local symmetries [4] (SLS), the shape is the union of ribbons using a line segment that varies in length along the axis.

We start with a simple 2D shape whose boundary is represented by a  $C^2$  continuous curve  $\alpha : \mathbb{I} \rightarrow \mathbb{R}^2$ , where  $\alpha$  and the domain  $\mathbb{I}$  are constructed to form an arc-length parameterization. Consider a line segment with end-points at  $\alpha(u)$  and  $\alpha(v)$  where  $u$  and  $v \in \mathbb{I}$  are parametric locations on the boundary curve—see Figure 3(a). The length of the

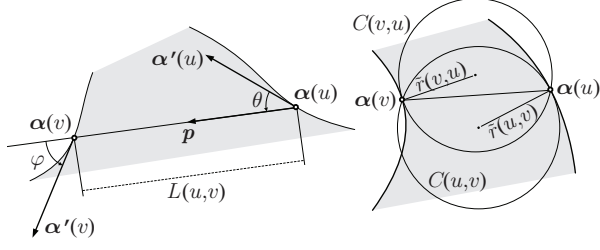


Figure 3. (a) Local geometry of a generator; (b) Partial tangent circles  $C(u, v)$  and  $C(v, u)$ .

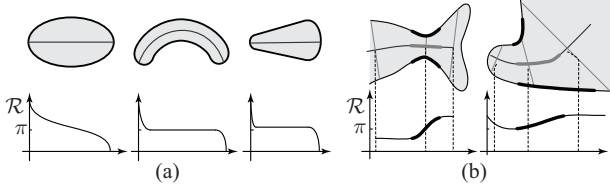


Figure 4. Shape and reliability profiles along symmetry axes

segment is simply  $L(u, v) = \|\alpha(v) - \alpha(u)\|$ , and its direction is  $\mathbf{p}(u, v) = \frac{1}{L(u, v)}(\alpha(v) - \alpha(u))$ . Our description of reliability will require the turning angle between the unit tangents at  $u$  and  $v$ , which are written  $\alpha'(u)$  and  $\alpha'(v)$ . Define the angle from  $\alpha'(u)$  to  $\mathbf{p}$  as  $\theta(u, v)$ , and the angle from  $\mathbf{p}$  to  $\alpha'(v)$  as  $\varphi(u, v)$ , where  $\theta, \varphi \in (-\pi, \pi]$ . Then, the total turning angle will just be  $\theta(u, v) + \varphi(u, v)$ . For the remainder of the paper, we assume  $(u, v)$  as the default parameters of these functions when the context is clear.

## 2.2. Making cuts

Later in Section 4.1 we will see that the reliability  $\mathcal{R}$  is defined as the total turning angle,  $\theta + \varphi$ . We can observe how  $\mathcal{R}$  changes as the line segment sweeps along the spine—in this case, we define the parameterization of the shape along the axis to be increasing in value as we move into the part.

We first look within a part. The top row of Figure 4(a) shows several planar primitives [6], while the second row of Figure 4(a) shows  $\mathcal{R}$ . In Figure 4(b), we give examples where the axis goes from one part into the other as well as the corresponding values of the reliability. We notice that the profiles of  $\mathcal{R}$  going across parts exhibit certain characteristics that we don't see within a part.

Within a part,  $\mathcal{R}$  starts at  $2\pi$  and is monotone non-increasing. When the axis leaves the body of one part and enters into another, it increases, until it totally enters into the other part. Thus, we can locate good places to cut by looking for where reliability increases quickly—where its derivative is positive and large. In the next section, we derive the expressions needed to make such measurements on shapes.

## 3. Differential Geometry of SLS

In this section, we will first study the differential properties of the length  $L$  and angles  $\theta$  and  $\varphi$  given any pair of points  $(u, v)$  on the curve. Then we limit the case when the two points form a local symmetry [4, 7]. Details of the derivations are provided in Appendix A.

### 3.1. Geometry of tangent circles

The partial tangent circle  $C(u, v)$  is the circle that is tangent to the curve at  $\alpha(u)$  and passes through  $\alpha(v)$ —its radius is  $\tilde{r}(u, v) = \frac{L}{2 \sin \theta}$ . See Figure 3(b). We can now state the partial derivatives of  $L$ ,  $\theta$  and  $\varphi$  with respect to  $u$  and  $v$ :

$$\nabla L = (-\cos \theta, \cos \varphi) \quad (1)$$

$$\begin{aligned} \nabla \theta &= \left( -\kappa(u) + \frac{1}{2\tilde{r}(u, v)}, \frac{1}{2\tilde{r}(v, u)} \right) \\ \nabla \varphi &= \left( -\frac{1}{2\tilde{r}(u, v)}, \kappa(v) - \frac{1}{2\tilde{r}(v, u)} \right), \end{aligned} \quad (2)$$

where  $\kappa$  is the curvature of  $\alpha$  (convex parts of the shape have positive curvature). Finally, we state the following, which will be relevant in describing symmetries:

$$\begin{aligned} \nabla(\theta + \varphi) &= (-\kappa(u), \kappa(v)) \\ \nabla(\theta - \varphi) &= \left( -\kappa(u) + \frac{1}{\tilde{r}(u, v)}, -\kappa(v) + \frac{1}{\tilde{r}(v, u)} \right). \end{aligned} \quad (3)$$

To formalize the mathematical form of the symmetry, we define the *asymmetry*  $\mathcal{A}(u, v)$  of  $u$  and  $v$  as the difference between  $\theta$  and  $\varphi$ , “wrapped” to the interval  $(-\pi, \pi]$ . Specifically,  $\mathcal{A}(u, v)$  is the angle in  $(-\pi, \pi]$  such that  $\sin \mathcal{A} = \sin(\theta - \varphi)$  and  $\cos \mathcal{A} = \cos(\theta - \varphi)$ . Two points  $\alpha(u)$  and  $\alpha(v)$  form a *symmetry pair* when  $\mathcal{A}(u, v) = 0$ , which is also known as a *local symmetry* by Brady and Asada [4]. They also define the loci of mid-points of symmetry pairs as *smoothed local symmetries* (SLS).

### 3.2. Geometry along symmetries

By definition, the motion of the two sides of the symmetry pair along the SLS is perpendicular to the gradient of the asymmetry  $\mathcal{A}$ . Suppose a small step ahead along the axis,  $ds$ , effects the parametric motion,  $du$  and  $dv$ , of the two sides, so that  $ds = \frac{1}{2}(\alpha'(u)du + \alpha'(v)dv)$ —see Figure 5. At a symmetry pair,  $\theta = \varphi$ ,  $\nabla \mathcal{A} \cdot (du, dv) = 0$  and  $r = \tilde{r}(u, v) = \tilde{r}(v, u)$ : the two partial tangent circles coincide with each other and form a bi-tangent circle, and we can relate  $du$  and  $dv$  as follows (derived in a different way by Giblin et al. [7]):

$$\left( \frac{1}{r} - \kappa(u) \right) du + \left( \frac{1}{r} - \kappa(v) \right) dv = 0. \quad (4)$$

For a normal symmetry axis, the two sides of the symmetry pair move along the curve boundary in opposite directions,

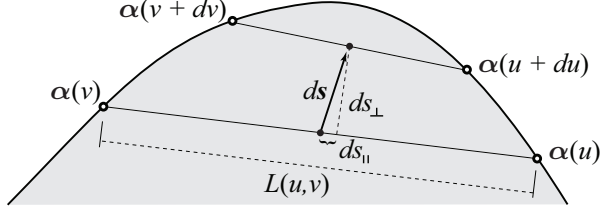


Figure 5. Local differential structure of the SLS axis

and thus  $du$  and  $dv$  have different signs. This occurs when  $(1/r - \kappa(u))$  and  $(1/r - \kappa(v))$  have the same sign [7], that is, the bi-tangent circle is either inscribe or circumscribe on both sides. Otherwise, the two sides will move along the curve in the same direction, resulting in a very unintuitive symmetry.

The step  $ds$  along the SLS axis can be decomposed into two components, which are measured perpendicular and parallel to  $\mathbf{p}$ , as in Figure 5:

$$ds_{\perp} = \frac{1}{2}(du - dv) \sin \theta, \quad ds_{\parallel} = \frac{1}{2}(du + dv) \cos \theta \quad (5)$$

Typically,  $\theta$  is far from zero and  $du$  and  $dv$  largely cancel each other when added. In this case, the parallel component  $ds_{\parallel}$  is very small compared with the perpendicular component  $ds_{\perp}$ . However, when  $\theta$  is close to zero,  $ds_{\parallel}$  can dominate the growth of the SLS axis, in which case, the symmetry axis does not intuitively reflect the symmetry structure of the shape. Thus, we only consider the perpendicular component  $ds_{\perp}$ . From (1) we can compute  $dL = \nabla L \cdot (du, dv) = (-du + dv) \cos \theta$ , and:

$$\frac{dL}{ds_{\perp}} = -2 \cot \theta. \quad (6)$$

## 4. Transitions between parts

We now describe how to compute the relatability in terms of local geometry along an SLS axis, show how it can be used to locate part transitions and assess their strength, and explain how it connects to and unifies existing approaches [23, 26].

### 4.1. Relatability

We are interested in the *relatability* between point  $\alpha(u)$  and  $\alpha(v)$  defined by  $\mathcal{R}(u, v) = \min_c \int_c |\kappa(\gamma)| d\gamma$ , where  $c$  is any interpolating curve connecting  $\alpha(u)$  and  $\alpha(v)$  [24]. For a curve parameterized by arc length and when  $\theta$  and  $\varphi$  are of the same sign (and thus are relatable), we can compute  $\mathcal{R}(u, v) = \theta + \varphi$ . Here we have adjusted the original definition from [24] so that perfect relatability is zero.

We can also find the change of relatability along the SLS given a small step  $ds$ . Given (3) and  $\theta = \varphi$ , we have  $d\mathcal{R} = -\kappa(u)du + \kappa(v)dv$ , and:

$$\frac{d\mathcal{R}}{ds_{\perp}} = -2 \csc \theta \frac{\kappa(u)w_u + \kappa(v)w_v}{w_u + w_v} \quad (7)$$

where  $w_u = 1/r - \kappa(v)$  and  $w_v = 1/r - \kappa(u)$ . From (7) we find that changes in relatability are determined by two quantities: the relatability, and a weighted average of curvatures measured at the symmetry pairs. Note that the sign of  $\frac{d\mathcal{R}}{ds_{\perp}}$  does not depend on the direction of  $ds$ . Finally, we note that the second derivative of  $L$  is proportional to the change of relatability. That is,

$$\frac{d^2L}{ds_{\perp}^2} = \csc^2 \theta \frac{d\mathcal{R}}{ds_{\perp}}. \quad (8)$$

Along smoothed local symmetries, a significant increase in relatability (a positive value of  $\frac{d\mathcal{R}}{ds_{\perp}}$ ) indicates a *transition* between parts: the crossing of a part boundary.

### 4.2. Transition strength

The value of (7) is scale dependent—it includes a curvature term. We can remove this scale dependence by multiplying it by  $r$ , the radius of the bi-tangent circle—this is proportional to the scale.

**Definition 4.1.** The *local strength of the part transition*,  $\mathcal{B}$ , of a symmetry pair is defined as the first derivative of relatability with respect to  $ds_{\perp}$ , normalized by the radius  $r$ :

$$\mathcal{B} = r \frac{d\mathcal{R}}{ds_{\perp}}.$$

A significant positive strength indicates a potential part transition. In practice, we employ a small positive threshold  $b$ . A useful range for  $b$  seems to be  $\frac{1}{5} \leq b \leq 1$ ; we use  $b = \frac{1}{2}$ .

When measuring the strength of an entire part transition, we cannot rely on individual points. For instance,  $\mathcal{B}$  could be spuriously large due to a sharp corner (in a polygonal approximation). Siddiqi et al. [23] measure the transition strength as the turning angle between the two nearby inflections. We cannot do this: our model of the part transition does not guarantee that two consecutive inflections are included (or that they even exist). Instead, we integrate the strength of the transition along the smoothed local symmetries that have  $\mathcal{B} > b$ . In this case, we integrate  $\frac{d\mathcal{R}}{ds_{\perp}}$  (without  $r$ ), because the length of the integration interval is scale dependent and will cancel the scale in  $\frac{d\mathcal{R}}{ds_{\perp}}$ . Such a measure is consistent with Hoffman and Singh's model of boundary strength, which equates the total turning angle at the boundary section to the turning angle at curvature minima [9]. This motivates the following definition:

**Definition 4.2.** The *total strength of a part transition*,  $\mathcal{T}$ , between two parts is defined as the change of relatability across the transitional section:

$$\mathcal{T} = \int_c \frac{d\mathcal{R}}{ds_{\perp}} ds_{\perp},$$

where  $c$  is the axis segment with  $\mathcal{B} > b$ .

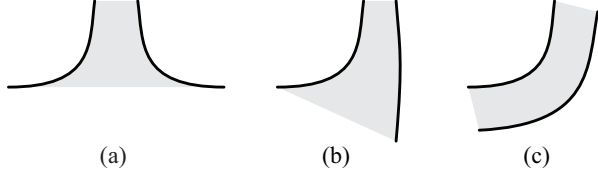


Figure 6. Limb transition (a); short-cut transition (b) and a bend (c). They share the same shape geometry and turning angle on the left side, so the boundary strength is determined by the right side.

By integrating (7), we consider the turning angle on *both* sides of the shape, which appropriately identifies transitions, and excludes other structures such as bends. Figure 6(a) shows the transitional region of a limb-based part—in this case, the curvatures on both sides add together and result in a large value of  $\mathcal{T}$ . This effectively implements the minima rule [8] for limbs and necks [23]. The strength  $\mathcal{T}$  of the short-cut in (b) is smaller—about half the strength of (a)—because only the curving side of the shape contributes. Thus, the same framework also implements the short-cut rule [26]. Finally, the bend in (c), which typically contains negative curvature minima, would have a very small value of  $\mathcal{T}$  as the terms from either side cancel. (Even though the concave side has higher curvature, the weights in (7) are larger on the outside.) This aspect of our model serves to explain why ligatures on bending structures can be considered as being within a coherent part [1], and are not a transition.

The implementation of the strength measure  $\mathcal{T}$  includes two stages of thresholding to identify a potential part cut. First, we locate continuous SLS segments that have significant local transitional strengths  $\mathcal{B} > b$ . Then for each of those sections,  $\mathcal{T}$  is computed—the transition is retained only when  $\mathcal{T}$  is above a threshold  $t$ . Useful values of  $t$  range from  $\frac{\pi}{8}$  to  $\frac{\pi}{4}$ ; we use  $t = \frac{\pi}{6}$ .

We examine the effects of varying of  $b$  and  $t$  on a range of shapes with similar structures in Figure 7. Figure 7(a) shows the effect of adjusting  $b$  for simple shapes with a *neck* transition. Each column of shapes is processed using the value of  $b$  on the top of the figure. As  $b$  is increased, the transition region between the shapes become smaller, and the shapes overlap more. Below each shape is the corresponding value of  $\mathcal{T}$  (divided by  $\pi$ ) for the transition. The necks are varied so they become less noticeable as one moves down the columns. The flattest necks on the bottom row are not detected for larger values of the threshold  $b$ . Figure 7(b) shows the same variation, but for shapes with a *short-cut* transition. As expected, the total strength values are a bit less than half of the value for the comparable example in (a).

Figure 8 demonstrates the algorithm for the detection of potential transitional areas along the leg of the kangaroo (seen later in Figure 11). The values of  $\mathcal{R}$  and  $\mathcal{B}$  are plotted on the right (with  $\mathcal{B}$  scaled by  $\tan^{-1}$ ). In this case, transition 2 is discarded since the value of  $\mathcal{T} < t$ .

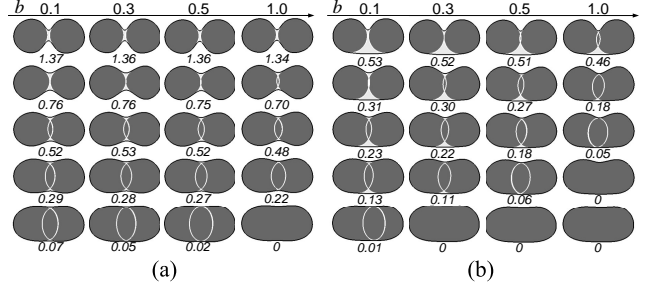


Figure 7. Effects of varying transition strength and  $b$ . Below each shape is the corresponding value of  $\mathcal{T}/\pi$  (or zero for no transition).

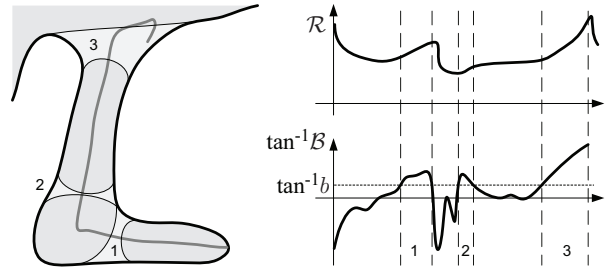


Figure 8. The reliability and the local strength along the SLS.

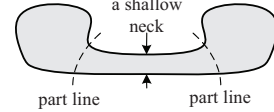


Figure 9. Shallow necks do not trigger part cuts

A neck is located at the symmetry pair where the generator has locally minimal length. That is,  $\frac{dL}{ds_{\perp}} = 0$  and  $\frac{d^2L}{ds_{\perp}^2} > 0$ . This means that necks are always potentially part cuts. However, if the neck is too shallow, then it does not give rise to a salient place to cut the shape. An example of a shallow neck is presented in Figure 9. The boundary strength  $\mathcal{B}$  is proportional to the curvatures, which corresponds to the notion of *curvature disparity* described by Siddiqi and Kimia [23]. Instead, in this case, this location is interpreted as a bend.

## 5. Implementation and Applications

### 5.1. Tracing SLS

Given a polygonal model with  $n$  vertices, identifying smoothed local symmetries by comparing each pair of vertices is quadratic in  $n$ . Here we introduce a more efficient algorithm to trace the symmetries of interest. We located the symmetries by detecting and tracing out zero crossings of  $\mathcal{A}$  in the  $(u, v)$  parameter space. We focus on zero crossings that terminate on the boundary of the shape. While this ignores cases where the SLS can form a closed loop [7], these symmetries do not correspond to potential part transitions and are safely overlooked. Our algorithm works with an  $n \times n$  grid (which wraps around at the boundaries).

The algorithm starts by locating zero crossings on the boundary at curvature extrema using the symmetry curvature duality theorem [17]. At a curvature-extremum vertex  $i$  with curve parameter  $u_i$ , we assume  $\mathcal{A}(u_i, u_i) = 0$ . Such endpoints are located on the diagonal of the grid. Then, we trace the zeros across the grid using a two-dimensional version of marching cubes [18]. Thus for the first step, we compute the other three corners of its adjacent grid points:  $\mathcal{A}(u_{i-1}, u_i)$ ,  $\mathcal{A}(u_i, u_{i+1})$  and  $\mathcal{A}(u_{i-1}, u_{i+1})$ . We find a zero crossing, and then move to the neighboring square across the edge that contains the zero. This procedure continues until we reach another boundary vertex—this must eventually occur [7]. In any square that crosses the SLS in the parameter space, there are usually two zero crossings along the four sides and the tracing can proceed unambiguously. For the case when a square contains four zero crossings, we choose the next edge in an anti-clockwise direction. Figure 10(a) shows the complete SLS for the kangaroo. Segments with  $\mathcal{B} > b$  are drawn with thicker lines. These segments include both peripheral transitional regions that are indicative of part boundaries as well as interior transitional regions that are not. In practice, we identify an initial set of *basic* parts by following the SLS from each curvature extremum. The algorithm stops whenever a section with total transitional strength above the threshold  $t$  is found. Thus, our algorithm can proceed without extracting the full SLS, but instead just those portions that describe the exterior parts.

## 5.2. Shape analysis by sequential deletion

Sequential pruning of basic parts is the typical approach to build a hierarchical description of a shape [20, 21, 23]. To eliminate dependence between scales, parts must be removed cleanly for correct analysis of the shape at coarser scales [21]. Identifying a transitional area between parts, naturally has this effect. When a part is deleted, we also delete the associated transitional area, leaving no trace of the part whatsoever. See Figure 10(b). We get one basic part by following the SLS from  $u_1$ . The part  $P_1$  is deleted by eliminating the entire transitional area from the SLS; we call this the *cutting boundary* of the part. The part itself incorporates none of the transitional area; what remains of the part when the transitional area is removed, together with the exterior boundary of the part, we call the *body line* of the part. In our implementation, we use a cubic Hermite curve to complete sections of the boundary of the part and the rest of the shape; other interpolation methods are possible [12].

A hierarchy is constructed by deleting the parts in a sequence. We prioritize the deleting order using the radius of bi-tangent circles along the SLS of the transition. Parts of the shape with smaller circles are removed first [13, 23]. Additionally, we group certain parts together and delete them simultaneously when they have similar radius

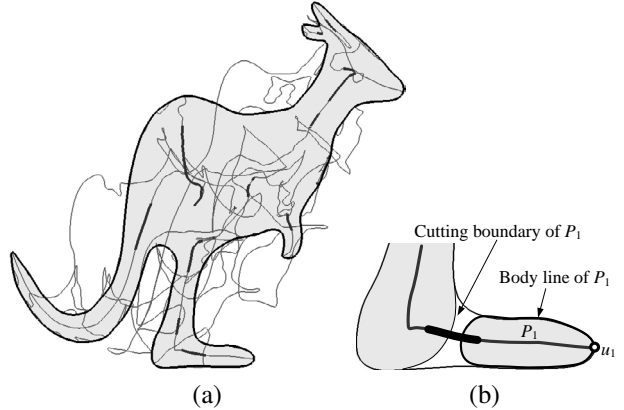


Figure 10. (a) The entire SLS—transitional regions are drawn with thicker lines; (b) Removing the foot—part  $P_1$ .

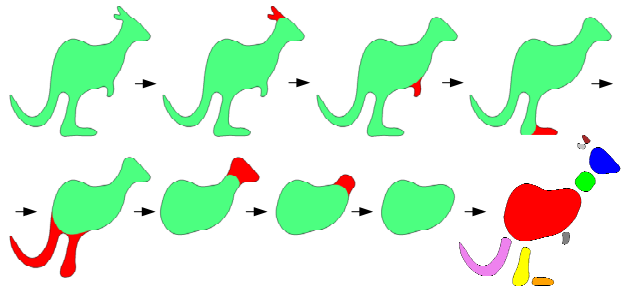


Figure 11. Sequentially deleting parts in the order of increasing radius of medial circles yields the components of a kangaroo shape

and area, and have intersecting transitional regions. We construct a common cutting boundary by fitting a NURBS curve through the intersections of the parts' cutting boundaries.

## 5.3. Results

Figure 11 shows the sequence of deletions that leads to the set of the components of the kangaroo shape. Figure 12 shows several more results. Note how the head and body of the elephant, and the wrist and palms of the hand, are actually analyzed as *overlapping* parts. Here the part arises from a transition region along the SLS that heads from the interior of the shape back towards the boundary. Perhaps surprisingly, the result remains intuitive—it recalls the artistic practice of defining shape by sketching overlapping masses. These cases underscore the conceptual distinction between our approach and traditional part-based segmentations.

Figure 13 offers an explicit comparison with the neck-based and limb-based parts proposed by Siddiqi and Kimia [23]. Again, we see that our approach is more flexible about the way it puts parts together—Siddiqi and Kimia have linear cuts only. This flexibility allows our system to find a range of natural parts that don't fit easily into a segmentation—the tail of the rabbit, the head and trunk of the elephant. It gives the parts themselves a simpler shape, as exemplified by the animals' bodies. And it means that we

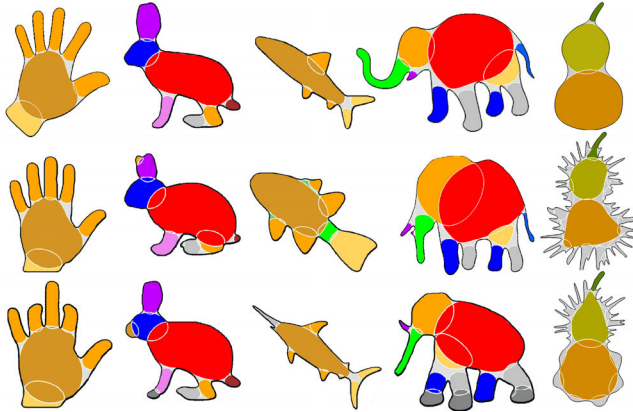


Figure 12. More results

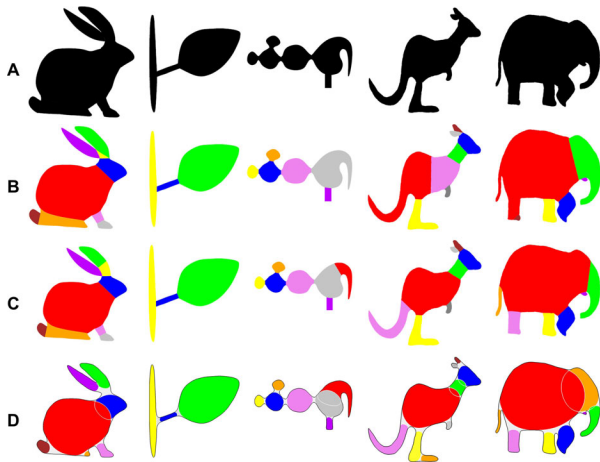


Figure 13. Decomposition examples. Row A contains five shapes from [23]. Row B shows decompositions into neck-based and limb-based parts [23]; Row C are the parts marked by human subjects [23]; Row D shows the results using our algorithm.

can find a wider range of parts with a single rule, including parts based on the short-cut rule [26] such as the tail of the elephant. Having this diverse array of parts opens up new applications in shape analysis.

## 6. Discussion and Conclusion

We have presented a new model for separating parts from 2D shapes, based on two cuts. We can cut the shape so what remains has the simplest possible structure. Alternatively, we can cut out the part so that the part itself takes on a simple shape. These cuts are different, but both can be characterized using the differential geometry of smoothed local symmetries and reliability. They do not directly give rise to a segmentation of the shape; a point inside the shape may associate with the part, the remainder, neither, or both.

Our work relies on an appropriate model of reliability, which is essentially a measure of contour grouping strength—we use a simple model from [24]. One avenue for improvement can come from studies on visual association

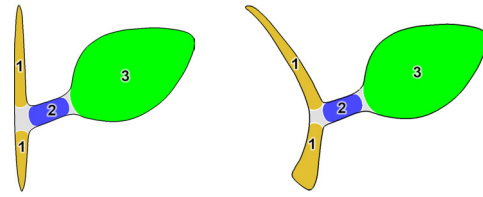


Figure 14. Ordering parts by radius can produce unintuitive results. (The numbers on the parts indicate deletion order.)

fields, which suggest that other geometric properties are relevant, such as the change in curvatures [12]. Psychophysical studies of 2D shape that explicitly represent transitions could also produce interesting findings. One possibility is to revisit the study by De Winter and Wagemans [5], and explicitly question the user about transition boundaries.

Section 5 shows how our model can be applied to compute the structural representation of a shape. However, the proposed method, which orders the deletion by the radius, can produce undesired results. Figure 14 shows two shapes with similar structure to the leaf example in the second column of Figure 13—in these examples, however, the stem is made thicker, so that the branch is deleted first. This results in the main branch being split (inappropriately) into two parts. Simple strategies that exclude transitions with non-negative curvatures work for the branch on the left, but not on the right. Thus, further investigations of disambiguating the part structure are necessary. We also intend to explore applications of our new part analysis in interfaces for sketching, manipulating and depicting shape.

## Acknowledgements

We thank Maneesh Agrawala, Manish Singh and Matthew Stone for their insights and helpful discussions. This work is partially supported by the National Science Foundation through grant CCF-0541185.

## References

- [1] J. August, K. Siddiqi, and S. W. Zucker. Ligature instabilities in the perceptual organization of shape. *CVIU*, 76(3):231–243, 1999.
- [2] H. Blum. Biological shape and visual science. *Journal of Theoretical Biology*, 38:205–287, 1973.
- [3] H. Blum and R. N. Nagel. Shape description using weighted symmetric axis features. *Pattern Recognition*, 10(3):167–180, 1978.
- [4] M. Brady and H. Asada. Smoothed local symmetries and their implementation. *Int. J. of Robotics Research*, 3:36–61, 1984.
- [5] J. De Winter and J. Wagemans. Segmentation of object outlines into parts: a large-scale integrative study. *Cognition*, 99(3):275–325, Apr 2006.
- [6] S. J. Dickinson, A. P. Pentland, and A. Rosenfeld. From volumes to views: an approach to 3-D object recognition.

In *IEEE Workshop on Directions in Automated CAD-Based Vision*, pages 85–96, 1991.

- [7] P. J. Giblin and S. A. Brassett. Local symmetry of plane curves. *The American Mathematical Monthly*, 92(10):689–707, Dec 1985.
- [8] D. D. Hoffman and W. Richards. Parts of recognition. *Cognition*, 18(1-3):65–96, Dec 1984.
- [9] D. D. Hoffman and M. Singh. Saliency of visual parts. *Cognition*, 63:29–78, 1997.
- [10] C. M. Hoffmann. *Geometric and Solid Modeling: An Introduction*. Morgan Kaufman, 1989.
- [11] P. J. Kellman and T. F. Shipley. A theory of visual interpolation in object perception. *Cognitive Psychology*, 23:141–221, 1991.
- [12] B. B. Kimia, I. Frankel, and A. Popescu. Euler spiral for shape completion. *IJCV*, 54(1-3):157–180, 2003.
- [13] B. B. Kimia, A. R. Tannenbaum, and S. W. Zucker. Shapes, shocks, and deformations I: the components of two-dimensional shape and the reaction-diffusion space. *IJCV*, 15(3):189–224, Jul 1995.
- [14] J. J. Koenderink and A. J. van Doorn. The shape of smooth objects and the way contours end. *Perception*, 11:129–137, 1982.
- [15] I. Kovács and B. Julesz. Perceptual sensitivity maps within globally defined visual shapes. *Nature*, 370:644–646, 1994.
- [16] L. J. Latecki and R. Lakmper. Convexity rule for shape decomposition based on discrete contour evolution. *CVIU*, 73(3):441–454, Mar 1999.
- [17] M. Leyton. Symmetry-curvature duality. *CVGIP*, 38:327–341, 1987.
- [18] W. E. Lorensen and H. E. Cline. Marching cubes: A high resolution 3D surface construction algorithm. In *SIGGRAPH 87*, pages 163–169, NY, USA, 1987. ACM Press.
- [19] S. Muraki. Volumetric shape description of range data using “blobby model”. In *SIGGRAPH 1991*, volume 25, pages 227–235, July 1991.
- [20] L. Prasad. Morphological analysis of shapes. *CNLS Newsletter*, 139, July 1997.
- [21] H. Rom and G. Medioni. Hierarchical decomposition and axial shape description. *IEEE PAMI*, 15(10):973–981, Oct 1993.
- [22] A. Rosenfeld. Axial representations of shape. *CVGIP*, 33(2):156–173, Feb 1986.
- [23] K. Siddiqi and B. B. Kimia. Parts of visual form: Computational aspects. *IEEE PAMI*, 17(3):239–251, 1995.
- [24] M. Singh and D. D. Hoffman. Completing visual contours: The relationship between relatability and minimizing inflections. *Perception & Psychophysics*, 61(5):943–951, 1999.
- [25] M. Singh and D. D. Hoffman. Part-based representations of visual shape and implications for visual cognition. In T. Shipley and P. Kellman, editors, *From fragments to objects: segmentation and grouping in vision, Advances in Psychology, Vol. 130*, pages 401–459. Elsevier, 2001.
- [26] M. Singh, G. D. Seyranian, and D. D. Hoffman. Parsing silhouettes: The short-cut rule. *Perception & Psychophysics*, 61:636–660, 1999.

## A. SLS Derivations

Section 3 provides a differential description of bitangent circles. Here, we derive  $\nabla\theta = (\partial\theta/\partial u, \partial\theta/\partial v)$  which is (2). We proceed by deriving  $\nabla \cos\theta = -\sin\theta \nabla\theta$  and solving for  $\nabla\theta$ :

$$\begin{aligned} \frac{\partial \cos\theta}{\partial u} &= \frac{\partial \alpha'(u) \cdot \mathbf{p}}{\partial u} = \frac{\partial \alpha'(u)}{\partial u} \cdot \mathbf{p} + \alpha'(u) \cdot \frac{\partial \mathbf{p}}{\partial u} \\ \frac{\partial \cos\theta}{\partial v} &= \frac{\partial \alpha'(u) \cdot \mathbf{p}}{\partial v} = \alpha'(u) \cdot \frac{\partial \mathbf{p}}{\partial v} \end{aligned}$$

Recall that  $\mathbf{p} = \frac{\alpha(v) - \alpha(u)}{\|\alpha(v) - \alpha(u)\|} = \frac{\alpha(v) - \alpha(u)}{L(u, v)}$ . It follows that:

$$\begin{aligned} \frac{\partial \|\alpha(v) - \alpha(u)\|}{\partial u} &= \frac{\partial \sqrt{(\alpha(v) - \alpha(u)) \cdot (\alpha(v) - \alpha(u))}}{\partial u} \\ &= -\alpha'(u) \cdot \mathbf{p} = -\cos\theta \\ \frac{\partial \|\alpha(v) - \alpha(u)\|}{\partial v} &= \alpha'(v) \cdot \mathbf{p} = \cos\varphi \end{aligned}$$

This is  $\nabla L$  from (1). Then, the derivatives of  $\mathbf{p}$  are:

$$\begin{aligned} \frac{\partial \mathbf{p}}{\partial u} &= \frac{(\alpha(v) - \alpha(u)) \cos\theta}{L(u, v)^2} - \frac{\alpha'(u)}{L(u, v)} = \frac{\mathbf{p} \cos\theta - \alpha'(u)}{L(u, v)} \\ \frac{\partial \mathbf{p}}{\partial v} &= \frac{-(\alpha(v) - \alpha(u)) \cos\varphi}{L(u, v)^2} + \frac{\alpha'(v)}{L(u, v)} = \frac{\alpha'(v) - \mathbf{p} \cos\varphi}{L(u, v)} \end{aligned}$$

We can also write  $\alpha'(u)$  in terms of the curvature  $\kappa(u)$ :

$$\frac{\partial \alpha'(u)}{\partial u} \cdot \mathbf{p} = \alpha''(u) \cdot \mathbf{p} = -\kappa(u) \mathbf{n}(u) \cdot \mathbf{p} = \kappa(u) \sin\theta$$

where  $\mathbf{n}(u)$  is the outward pointing normal vector at  $u$ . Given that  $\tilde{r}(u, v) = \frac{L(u, v)}{2 \sin\theta}$  and  $\tilde{r}(v, u) = \frac{L(u, v)}{2 \sin\varphi}$ , we can determine the components of  $\nabla\theta$ :

$$\begin{aligned} \frac{\partial \theta}{\partial u} &= \frac{1}{-\sin\theta} \left( \kappa(u) \sin\theta + \frac{\cos^2\theta - 1}{L(u, v)} \right) = -\kappa(u) + \frac{1}{2\tilde{r}(u, v)} \\ \frac{\partial \theta}{\partial v} &= \frac{1}{-\sin\theta} \left( \frac{\cos(\theta + \varphi) - \cos\theta \cos\varphi}{L(u, v)} \right) = \frac{1}{2\tilde{r}(v, u)} \end{aligned}$$

which is the first part of (2). To derive  $\nabla\varphi$ , we consider the other side of  $\mathbf{p}$  in Figure 3 and use the form of  $\nabla\theta$ . This yields  $\frac{\partial(\pi - \varphi)}{\partial v} = -\kappa(v) + \frac{1}{2\tilde{r}(v, u)}$ . Thus,

$$\frac{\partial \varphi}{\partial u} = -\frac{1}{2\tilde{r}(u, v)}, \quad \frac{\partial \varphi}{\partial v} = \kappa(v) - \frac{1}{2\tilde{r}(v, u)}.$$